

Charge and spin manipulation in a few-electron double dot

J. R. Petta^{a,1}, A. C. Johnson^a, J. M. Taylor^a, A. Yacoby^b, M. D. Lukin^a, C. M. Marcus^a,
M. P. Hanson^c, and A. C. Gossard^c,

^a*Department of Physics, Harvard University, Cambridge, MA 02138*

^b*Department of Condensed Matter Physics, Weizmann Institute of Science, Rehovot 76100 Israel*

^c*Materials Department, University of California, Santa Barbara, CA 93106*

Abstract

We demonstrate high speed manipulation of a few-electron double quantum dot. In the one-electron regime, the double dot forms a charge qubit. Microwaves are used drive transitions between the (1,0) and (0,1) charge states of the double dot. A local quantum point contact charge detector measures the photon-induced change in occupancy of the charge states. Charge detection is used to measure $T_1 \sim 16$ ns and also provides a lower bound estimate for T_2^* of 400 ps for the charge qubit. In the two-electron regime we use pulsed-gate techniques to measure the singlet-triplet relaxation time for nearly-degenerate spin states. These experiments demonstrate that the hyperfine interaction leads to fast spin relaxation at low magnetic fields. Finally, we discuss how two-electron spin states can be used to form a logical spin qubit.

Key words: charge qubit, spin qubit, Rabi oscillation, coherent manipulation

PACS: 03.67.Mn, 72.25.Rb, 85.35.Gv

Semiconducting quantum dots can be used to confine single electrons in an electrically controllable potential [1]. Coupled quantum dots, containing a single electron, create a tunable two-level system for the manipulation of single charges [2,3]. By a similar approach, when two electrons are confined to a double dot the relaxation and dephasing of singlet and triplet spin states can be studied [4,5,6]. Recently, we have demonstrated coherent control of two-electron spin states by using high speed pulsed gate techniques [7]. In this paper, we review recent experiments performed by our group on few-electron quantum dots that demonstrate quantum control of just one or two electrons [3,5,6,7,8].

Samples are fabricated from a GaAs/Al_{0.3}Ga_{0.7}As heterostructure grown by molecular beam epitaxy (Fig. 1(a)). Electron beam lithography and liftoff techniques are used to fabricate Ti/Au gates, which deplete the two-dimensional electron gas with electron density $2 \times 10^{11} \text{ cm}^{-2}$ and mobility $2 \times 10^5 \text{ cm}^2/\text{V}\cdot\text{s}$. When the gates are appropriately biased a double well potential is formed. The electron number in the left(right) dot is varied by tuning $V_L(V_R)$. Interdot tunnel coupling is tuned by changing the voltage V_T . Standard lock-in techniques are used to measure the double dot conductance, G_D , and the quantum point contact (QPC) conductances, $G_{S1(S2)}$. The sample is cooled to base temperature in a dilution refrigerator with an electron temperature, $T_e \sim 135$ mK, as determined from Coulomb blockade peak widths. Depend-

¹ Corresponding author. E-mail: petta@deas.harvard.edu

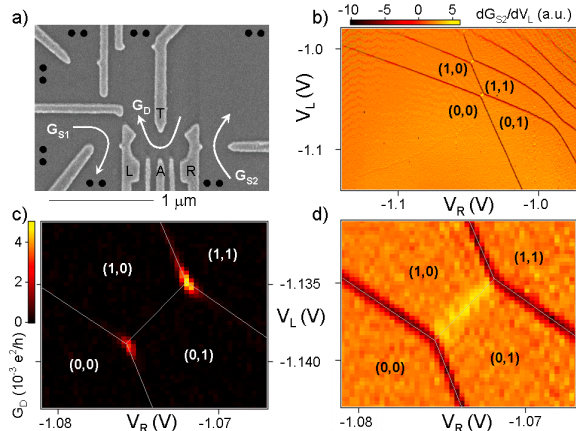


Fig. 1. Transport and charge sensing of a few-electron double dot. (a) Scanning electron microscope (SEM) image of a double dot device similar to the one used in these experiments. The double dot is flanked by two QPC charge detectors. Gates L(R) primarily change the number of electrons in the left(right) dot. Interdot tunnel coupling can easily be tuned by adjusting the voltage on gate T. \bullet denotes an Ohmic contact. The double dot conductance, G_D , and the QPC conductances, G_{S1} and G_{S2} , are measured using standard lock-in techniques. (b) Large scale plot of dG_{S2}/dV_L as a function of V_R and V_L . Charge states are labelled (M,N) , where $M(N)$ is the time averaged number of electrons on the left (right) dot. G_D , in (c), and dG_{S2}/dV_L , in (d), as a function of V_R and V_L near the $(1,0)$ to $(0,1)$ transition. The gates have been slightly adjusted in (c-d) relative to (b) to allow simultaneous transport and sensing. Identical color-scales are used in (b) and (d).

ing on the experimental arrangement continuous-wave (cw) microwaves are applied to gate A, or high speed pulses are applied to gates L and R using bias tees [9] that are thermally anchored to the mixing chamber.

1. Isolating single charges

Control of the double dot using dc gate voltages is demonstrated in Fig. 1 (b-d). Figure 1(b) shows dG_{S2}/dV_L (numerically differentiated) as a function of V_R and V_L . When an electron enters or leaves the double dot, or moves from one dot to the other, the QPC conductance changes. Gate voltage derivatives of G_{S1} and G_{S2} clearly show these changes and map out the double dot charge stability diagram [10,11]. The nearly horizontal lines are due to charge transitions in the left dot, while the nearly vertical lines correspond to charge

transitions in the right dot. For very negative values of V_L and V_R (see the lower left corner of the charge stability diagram) charge transitions no longer occur, indicating that the double dot is completely empty, denoted $(0,0)$. Transport through the double dot can be correlated with simultaneous charge sensing measurements. Figure 1(c) shows a color scale plot of G_D near the $(1,0)$ to $(0,1)$ charge transition. A charge stability diagram, simultaneously acquired, is shown in Fig. 1(d). Near the $(1,0)$ to $(0,1)$ charge transition the system behaves as an effective two-level system. Crossing this transition by making V_L more positive transfers a single electron from the right dot to the left dot.

2. Microwave manipulation of a single charge

Near the $(0,1)$ to $(1,0)$ interdot transition, the double dot forms a two-level charge system that can be characterized by the detuning parameter, ϵ , and the tunnel coupling, t (see inset of Fig. 2(b)) [12]. We have used microwave spectroscopy to characterize this two-level system [3]. Microwaves drive transitions in the double dot when the photon frequency is equal to the energy separation between the $(1,0)$ and $(0,1)$ charge states [13,14,15]. This microwave-induced charge state repopulation can be directly measured using the QPC charge sensors [16,17]. The black curve in Fig. 2(a) shows the measured charge on the left dot, M , as a function of ϵ , in the absence of microwave excitation. As expected, increasing ϵ transfers a single charge from the left dot to the right dot. Application of microwaves to gate A results in resonant peaks in M vs. ϵ that move to larger $|\epsilon|$ with increasing frequency. This resonant peak corresponds to a single photon process that drives an electron from the $(1,0)$ ground state (for negative ϵ) into the $(0,1)$ excited state, or vice versa.

The frequency dependence of the resonance condition can be used to map out the energetics of the charge two-level system. Detailed measurements of the resonant peak position as a function of microwave frequency, f , are used to extract t for various V_T (see Fig. 2(b)) [18]. At high frequencies the peak positions move linearly with f . For small frequencies, probing the region near the $(0,1)$ - $(1,0)$ charge transition, the interdot tunnel coupling modifies the linear dependence. Changing the interdot tunnel coupling modifies the fre-

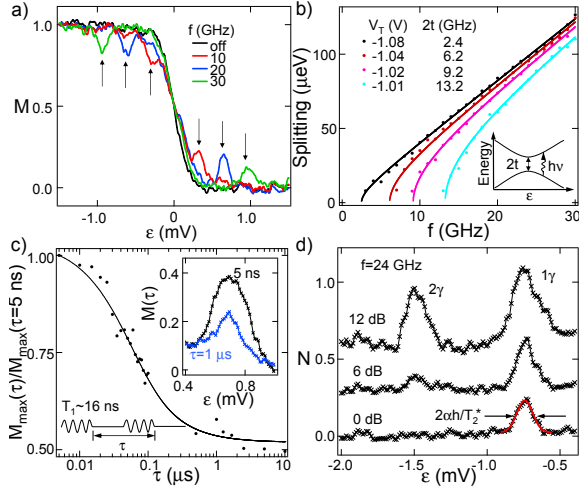


Fig. 2. Microwave spectroscopy of a one-electron double dot. (a) Charge occupancy of the left dot, M , as a function of ϵ for several microwave frequencies. (b) One-half of the resonance peak splitting as a function of f for several values of V_T . Solid lines are best fits to the experimental data using the theory outlined in the text. Inset: two-level system energy level diagram. (c) Amplitude of the resonance, expressed as $M_{\text{max}}(\tau)/M_{\text{max}}(\tau=5 \text{ ns})$, as a function of chopped cw period, τ , with $f=19 \text{ GHz}$. Theory gives a best fit $T_1=16 \text{ ns}$ (solid line, see text). Inset: Single photon peak shown in a plot of M as a function of ϵ for $\tau=5 \text{ ns}$ and $1 \mu\text{s}$. (d) Power dependence of the resonance for $f=24 \text{ GHz}$. Widths are used to extract the ensemble-averaged charge dephasing time T_2^* . At higher microwave powers multiple photon processes occur. Curves are offset by 0.3 for clarity.

quency dependence of the resonant peak position. For each value of V_T , the experimental data have been fit using $\alpha\epsilon = \sqrt{(hf)^2 - (2t)^2}$, where α is the lever arm. α and t were used as free parameters for each curve. The lever arm α changes by $\sim 20\%$ over the range of V_T used in Fig. 2. The experimental data are well fit by theory and show that the tunnel coupling varies by roughly a factor of 6 when V_T is changed by 70 mV. Measurements of t from microwave spectroscopy are consistent with values obtained by measuring the width of the interdot charge transition using charge sensing [19,3].

Charge relaxation and decoherence times can be extracted by analyzing the resonant response of the two-level system, as used in the analysis of the Cooper pair box [17]. The charge relaxation time T_1 is determined by measuring the resonance peak height as microwaves are chopped at varying periods, τ , with a 50% duty cycle [20]. The system response is modelled with a satu-

rated signal while microwaves are present, followed by an exponential decay with a characteristic time scale T_1 when the microwaves are turned off. Calculating the time averaged occupation, we expect:

$$\frac{M_{\text{max}}(\tau)}{M_{\text{max}}(0)} = \frac{1}{2} + \frac{T_1(1 - e^{-\tau/(2T_1)})}{\tau} \quad (1)$$

With long periods ($\tau \gg T_1$), the exponential tail due to the finite relaxation time is an insignificant part of the duty cycle, and the charge detector measures the time average of the on/off signal, giving a resonant feature with half the height found in the limit $\tau \rightarrow 0$. When the period is very short, such that $\tau \ll T_1$, the charge has little time to relax, and the charge detector response is close to saturation (saturation is defined as $M_{\text{max}}=0.5$ on resonance). In the intermediate regime where $\tau \sim T_1$, the QPC signal is strongly dependent on τ . We present data for $\tau \geq 5 \text{ ns}$ to avoid artifacts due to the finite rise time of the mixer circuit. In Fig. 2(c), we plot $M_{\text{max}}(\tau)/M_{\text{max}}(\tau=5 \text{ ns})$ as a function of τ . Agreement between experiment and theory is good and gives a best fit $T_1=16 \text{ ns}$.

The resonance peak width gives a direct measure of the inhomogeneous charge decoherence time, T_2^* [17,21]. In Fig. 2(d) we plot N as a function of ϵ for several microwave powers. At low power, only the single-photon (1γ) peak is visible. As the power is increased the 1γ peak approaches saturation and a two-photon peak develops [22]. A fit to the low power 1γ peak using a Gaussian function is shown in red in Fig. 2(d). The best fit half-width of 0.077 mV corresponds to an energy of $10.2 \mu\text{eV}$ when taking into account the lever arm. Converting this into a time results in a lower bound $T_2^*=400 \text{ ps}$. This measurement of T_2^* gives a worst-case estimate since charge fluctuations will broaden the resonant feature, resulting in a shorter T_2^* value.

Our measurements of T_1 and T_2^* using charge sensing can be compared with other recent experiments [2,23]. In a pulsed-gate experiment, Fujisawa *et al.* [23] have measured the energy relaxation time in a vertical quantum dot. From a measurement of the transient current as a function of pulse time they extract $T_1=10 \text{ ns}$, which is limited by spontaneous emission of a phonon. Direct observation of coherent charge oscillations has been reported by Hayashi *et al.* [2]. From the decay envelope of the Rabi oscillations Hayashi *et al.* extract a T_2 time of $\sim 1 \text{ ns}$, which serves as an up-

per bound estimate for T_2^* . The T_1 and T_2^* values that we obtain from charge sensing are in good agreement with the results of these previous experiments.

3. Triplet-singlet spin relaxation

Spin physics can be studied in the one-electron regime at high fields, where the spin-up and spin-down states are separated by the Zeeman splitting, or in the two-electron regime with singlet and triplet spin states. We focus on the two-electron regime, where differences in the singlet-triplet splittings in the (1,1) and (0,2) charge states can be put to use for spin state readout and initialization. We show that singlet-triplet relaxation times can be measured by implementing a charge pump experiment in the two-electron regime. This measurement technique can be used to measure the singlet-triplet relaxation time, τ_{ST} , for nearly degenerate singlet and triplet states, a regime in which hyperfine mediated relaxation processes are expected to be important.

In the two-electron regime, charge transport in a double dot shows a striking asymmetry in bias voltage due to spin selection rules (Pauli blocking) [4,8]. The asymmetry in charge transport is due to the large difference in the singlet-triplet splittings for the (1,1) and (0,2) charge states. In the weakly-coupled (1,1) charge configuration the singlet and triplet states are nearly degenerate. However, two tightly confined electrons in the (0,2) charge state result in a singlet-triplet splitting $J \sim 400 \mu\text{eV}$. At forward bias, transitions from the (0,2) singlet state, $(0,2)_S$, to the (1,1) singlet state, $(1,1)_S$, are allowed. However, reverse bias (1,1) to (0,2) charge transitions are blocked if the (1,1) state forms a triplet $(1,1)_T$ because the $(0,2)_T$ state resides outside the transport window due to the large singlet-triplet splitting in (0,2). This asymmetry results in current rectification, which can be used for spin-to-charge conversion and spin state readout.

Charge transitions are driven by applying pulses to gates L and R. Experimental details concerning pulse calibration have been previously published [5]. In double dots, charge can be pumped by pulsing gates around a triple point, e.g. $(0,1) \rightarrow (1,1) \rightarrow (0,2) \rightarrow (0,1)$. Our spin relaxation measurement technique relies on the fact that $(1,1)_T$ to $(0,2)_S$ transitions are spin blocked. Mea-

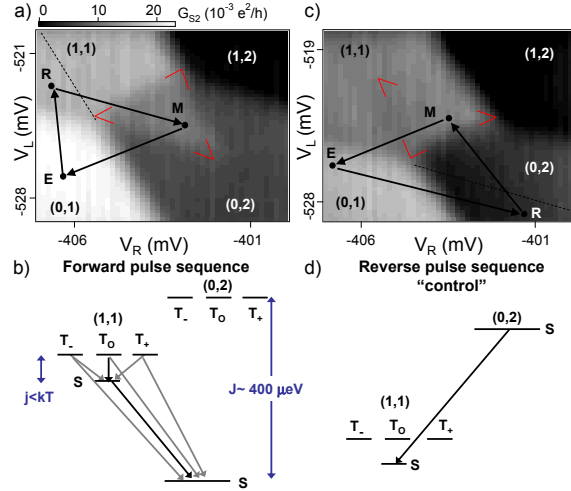


Fig. 3. Pulse gate techniques for measuring the singlet-triplet relaxation time. (a) G_{S2} , as a function of V_L and V_R , measured while applying the forward pulse sequence $(0,1) \rightarrow (1,1) \rightarrow (0,2) \rightarrow (0,1)$. The pulse period $\tau = 10 \mu\text{s}$ and the perpendicular field $B_{\perp} = 100 \text{ mT}$. We observe a charge sensing signal in the pulse triangle (bounded by the red lines) that takes on a value between the raw (1,1) and (0,2) signal levels. This signal is indicative of spin-blocked charge transitions. Outside of the pulse triangle, transitions through the (1,2) and (0,1) charge states are possible and relax the spin blockade. (b) Energy level diagram illustrating the possible transitions from (1,1) to (0,2). Fast transitions are indicated with black arrows, spin blocked transitions with grey arrows. (c) G_{S2} as a function of V_L and V_R while applying the reverse “control” pulse sequence, $(0,1) \rightarrow (0,2) \rightarrow (1,1) \rightarrow (0,1)$. The pulse period $\tau = 10 \mu\text{s}$ and the perpendicular field $B_{\perp} = 100 \text{ mT}$. The $(0,2)_S$ to $(1,1)_S$ transition is not spin blocked and as a result, there is no detectable pulse signal in the pulse triangle (bounded by the red lines). (d) Level diagram illustrating the (0,2) to (1,1) transition. A best-fit plane has been subtracted from the data in (a),(c) to remove signal from direct gate to QPC coupling.

asuring this charge transition probability as a function of time using charge sensing allows a measurement of the spin relaxation time. We demonstrate that the observed time dependence of the charge sensing signal is due to spin blocked transitions.

The pulse sequence used to measure τ_{ST} is shown in [Fig. 3(a)]. The gates are held at point E for 10% of the period, emptying the second electron from the double dot, leaving the (0,1) charge state. A pulse shifts the gates to point R (reset point) for the next 10% of the period. This initializes the system into the (1,1) configuration. Since the singlet and triplet states are nearly

degenerate in (1,1) we expect to load into (1,1)_S or any of the three (1,1)_T states with equal probability. For the final 80% of the period, the gates are held at the measurement point M where (0,2)_S is the ground state. The energetics of the spin states at the measurement point are shown in Fig. 3(b). A (1,1)_S state prepared in the R step will tunnel to (0,2)_S on a timescale set by the interdot tunneling rate, $\Gamma(\epsilon)$. The $m_s=0$ (1,1) triplet state, (1,1)_{T0}, will dephase into (1,1)_S on a timescale set by T_2 (expected to be ≤ 100 ns [24,25,26]) followed by a direct transition to (0,2)_S. Roughly half of the time the R step will load the $m_s=1$ (1,1) triplet state, (1,1)_{T+}, or the $m_s=-1$ (1,1) triplet state, (1,1)_{T-}. Since (0,2)_T is inaccessible a transition from (1,1)_{T+} or (1,1)_{T-} to (0,2) requires a spin flip and will be blocked for times shorter than the singlet-triplet relaxation time τ_{ST} .

Figure 3(a) shows the time-averaged charge sensor conductance G_{S2} , measured as a function of the dc gate voltages V_L and V_R , while the forward pulse sequence is repeated. The conductance G_{S2} maps out the ground state population at point M since 80% of the duty cycle is spent there. The plateaus in G_{S2} at ~ 0.0 , 6.0, 16, and $23 \times 10^{-3} e^2/h$ indicate full population of the (1,2), (0,2), (1,1), and (0,1) charge states respectively. The pulse data differs from ground state data only when point M resides in the triangle defined by the (1,1) to (0,2) ground state transition and the extensions of the (1,1) to (0,1) and (1,1) to (1,2) ground state transitions (bounded by the red marks in Fig. 3(a)). Inside of the “pulse triangle” transitions from (1,1) to (0,2) may be spin-blocked and the charge sensor registers a conductance intermediate between the (1,1) and (0,2) plateaus. Outside of the pulse triangle it is possible to access (0,1) or (1,2), which relaxes the spin blockade. Figure 3(a) shows a signal of $11 \times 10^{-3} e^2/h$ in the pulse triangle for $\tau=10 \mu s$, indicating that approximately 50% of the time the dots remain in (1,1) even though (0,2) is the ground state. This is direct evidence of spin-blocked (1,1) to (0,2) transitions.

To check that the pulse signal is due to spin-blocked transitions and not just a slow interdot tunnel rate we compare the forward pulse sequence with a reverse pulse sequence that does not involve spin selective transitions [(0,1) \rightarrow (0,2) \rightarrow (1,1) \rightarrow (0,1)]. In the reverse pulse sequence the reset position R occurs in (0,2) where only the singlet state is accessible, and M occurs in (1,1). Now tunneling from R to M should always proceed on a time scale set by the interdot tunnel coupling, since

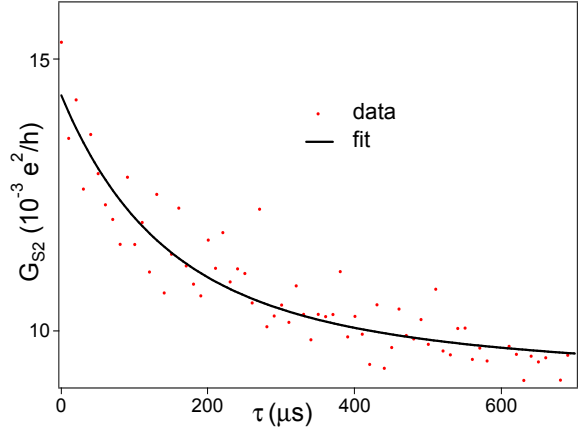


Fig. 4. Time dependence of the spin-blocked signal. G_{S2} measured as a function of τ . In the (0,2) charge state $G_{S2}=10 \times 10^{-3} e^2/h$, while $G_{S2}=20 \times 10^{-3} e^2/h$ in the (1,1) charge state. For short τ , the (1,1) to (0,2) transition is blocked approximately half of the time, resulting in a pulse signal of $15 \times 10^{-3} e^2/h$ in the (0,2) pulse triangle. The (1,1) to (0,2) transition probability increases (sensor signal decreases) with τ due to spin-relaxation with a characteristic time scale of $70 \pm 10 \mu s$. A best-fit plane has been subtracted from the data.

the (0,2)_S to (1,1)_S transition is not spin blocked. No signal is seen in the pulse triangle for this reversed “control” sequence (Fig. 3(c)).

The singlet-triplet relaxation time can be determined by measuring the time dependence of the charge sensing signal inside of the pulse triangle. We extract τ_{ST} by measuring G_{S2} as a function of the pulse train period, τ . G_{S2} is measured inside the pulse triangle (V_R, V_L held fixed at -403, -523.8 mV, respectively) and is plotted as a function of τ in Fig. 4. In (1,1), $G_{S2} \sim 20 \times 10^{-3} e^2/h$, whereas outside the pulse triangle in (0,2), $G_{S2} \sim 10 \times 10^{-3} e^2/h$. For small τ , $G_S \sim 15 \times 10^{-3} e^2/h$ in the pulse triangle. At long τ , G_S approaches $10 \times 10^{-3} e^2/h$ in the pulse triangle, which indicates complete transfer from the (1,1) to (0,2) charge state. We fit these experimental data assuming exponential singlet-triplet relaxation and find a best fit $\tau_{ST}=70 \pm 10 \mu s$. The dependence of the singlet-triplet relaxation time on detuning and magnetic field has been presented in [6]. A speed up of spin relaxation near zero field is observed and is consistent with a hyperfine mediated spin relaxation process.

4. Coherent spin manipulation

With an external magnetic field applied so that the $m_s = \pm 1$ triplet states are split off, the $(1, 1)_S$ and $(1, 1)_{T0}$ states form a logical qubit. Due to the large singlet triplet splitting in $(0, 2)$ we can easily initialize the system in $(0, 2)_S$. $(0, 2)_S$ can be transferred to $(1, 1)_S$ by sweeping the detuning adiabatically with respect to the interdot tunnel coupling. The $(1, 1)_S$ and $(0, 2)_S$ states are hybridized at zero detuning due to the interdot tunnel coupling. This hybridization results in an exchange splitting between the $(1, 1)_S$ and $(1, 1)_{T0}$ states, $j(\epsilon)$. For large negative detunings, $j(\epsilon) \rightarrow 0$. The exchange $j(\epsilon)$ can be tuned on ns timescales by applying pulses to the gates defining the double dot. Using this fast control of the exchange energy we have recently implemented a spin SWAP operation [7].

We acknowledge useful discussions with Sankar Das Sarma, Hans-Andreas Engel, Xuedong Hu, Daniel Loss, Emmanuel Rashba, and Peter Zoller. Funding was provided through the ARO under DAAD55-98-1-0270 and DAAD19-02-1-0070, the DARPA-QuIST program, and the NSF under DMR-0072777, the Harvard Center for Nanoscale Systems, and the Sloan and Packard Foundations.

References

- [1] M. Ciorga *et al.*, Phys. Rev. B **61**, 16315 (2000).
- [2] T. Hayashi *et al.*, Phys. Rev. Lett., **91**, 226804 (2003).
- [3] J. R. Petta *et al.*, Phys. Rev. Lett. **93**, 186802 (2004).
- [4] K. Ono *et al.*, Science **297**, 1313 (2002).
- [5] J. R. Petta *et al.*, Phys. Rev. B **72**, 161301(R) (2005).
- [6] A. C. Johnson *et al.*, Nature **435**, 925 (2005).
- [7] J. R. Petta *et al.*, Science **309**, 2180 (2005).
- [8] A. C. Johnson *et al.*, Phys. Rev. B **72**, 165308 (2005).
- [9] Anritsu Company, Model K251.
- [10] M. Field *et al.*, Phys. Rev. Lett. **70**, 1311 (1993).
- [11] J. M. Elzerman *et al.*, Phys. Rev. B **67**, 161308 (2003).
- [12] W. G. van der Wiel *et al.*, Rev. Mod. Phys. **75**, 1 (2003).
- [13] C. A. Stafford and N. S. Wingreen, Phys. Rev. Lett. **76**, 1916 (1996).
- [14] T. H. Stoof and Y. V. Nazarov, Phys. Rev. B **53**, 1050 (1996).
- [15] P. Brune, C. Bruder, H. Schoeller, Phys. Rev. B **56**, 4730 (1997).
- [16] C. H. van der Wal *et al.*, Science **2000**, 290 (2000).
- [17] K. W. Lehnert *et al.*, Phys. Rev. Lett. **90**, 027002 (2003).
- [18] T. H. Oosterkamp *et al.*, Nature **395**, 873 (1998).
- [19] L. DiCarlo *et al.*, Phys. Rev. Lett. **92** 226801 (2004).
- [20] Marki Microwave, Model MM8-0420MS-00.
- [21] A. Abragam, *The Principles of Nuclear Magnetism: The International Series of Monographs on Physics 32* (Oxford University Press, Oxford, 1983).
- [22] We have occasionally observed peak heights exceeding saturation, implying microwave induced population inversion. (Petta, Johnson, Marcus, Hanson, Gossard) unpublished.
- [23] T. Fujisawa *et al.*, Nature, **419**, 278 (2002).
- [24] J. M. Kikkawa and D. D. Awschalom, Phys. Rev. Lett. **80**, 4313 (1998).
- [25] A. V. Khaetskii, D. Loss, L. Glazman, Phys. Rev. Lett. **88**, 186802 (2002).
- [26] I. A. Merkulov, Al. L. Efros, M. Rosen, Phys. Rev. B **65**, 205309 (2002).